Tryptophan metabolism and bacterial commensals prevent fungal dysbiosis in *Arabidopsis* roots

Katarzyna W. Wolinska[a], Nathan Vannier[a], Thorsten Thiergart[a], Brigitte Pickel[a], Sjoerd Gremmen[a], Anna Piasecka[b], Mariola Piślewska-Bednarek[b], Ryohei Thomas Nakano[a], Youssef Belkhadir[c], Paweł Bednarek[b], and Stéphane Hacquard[a,d,1]

[a]Department of Plant Microbe Interactions, Max Planck Institute for Plant Breeding Research, 50829 Cologne, Germany; [b]Institute of Bioorganic Chemistry, Polish Academy of Sciences, 61-704 Poznań, Poland; [c]Gregor Mendel Institute, Austrian Academy of Sciences, Vienna Biocenter, 1030 Vienna, Austria; and [d]Cluster of Excellence on Plant Sciences, Max Planck Institute for Plant Breeding Research, 50829 Cologne, Germany

Edited by Jeffery L. Dangl, University of North Carolina at Chapel Hill, Chapel Hill, NC, and approved October 27, 2021 (received for review June 22, 2021)

In nature, roots of healthy plants are colonized by multikingdom microbial communities that include bacteria, fungi, and oomycetes. A key question is how plants control the assembly of these diverse microbes in roots to maintain host–microbe homeostasis and health. Using microbiota reconstitution experiments with a set of immunocompromised *Arabidopsis thaliana* mutants and a multikingdom synthetic microbial community (SynCom) representative of the natural *A. thaliana* root microbiota, we observed that microbiota-mediated plant growth promotion was abolished in most of the tested immunocompromised mutants. Notably, more than 40% of between-genotype variation in these microbiota-induced growth differences was explained by fungal but not bacterial or oomycete load in roots. Extensive fungal overgrowth in roots and altered plant growth was evident at both vegetative and reproductive stages for a mutant impaired in the production of tryptophan-derived, specialized metabolites (*cyp79b2/b3*). Microbiota manipulation experiments with single- and multikingdom microbial SynComs further demonstrated that 1) the presence of fungi in the multikingdom SynCom was the direct cause of the dysbiotic phenotype in the *cyp79b2/b3* mutant and 2) bacterial commensals and host tryptophan metabolism are both necessary to control fungal load, thereby promoting *A. thaliana* growth and survival. Our results indicate that protective activities of bacterial root commensals are as critical as the host tryptophan metabolic pathway in preventing fungal dysbiosis in the *A. thaliana* root endosphere.

plant innate immunity | microbial homeostasis | microbial interactions | root microbiome | plant holobiont

Roots of healthy plants are colonized by a staggering diversity of microbes, including bacteria, fungi, and oomycetes, forming complex multikingdom microbial communities that affect plant productivity [i.e., the root microbiota (1–4)]. Paradoxically, plants have evolved a complex multilayer immune system that detects microbial invasion and discriminates self from nonself (5–8). A first line of defense, referred to as pattern-triggered immunity (PTI), comprises membrane-localized receptors and associated coreceptors, which coordinately detect microbe/damage-associated molecular patterns (8) and initiate downstream defense responses (9), leading to the biosynthesis of phytohormones (10) and plant-specialized metabolites that restrict pathogen growth in planta (11).

Although the plant innate immune system has been extensively studied under laboratory conditions, typically in leaves upon inoculation with particular host-adapted microbial pathogens, our understanding of this complex machinery in accommodating commensal microbes in roots and in maintaining host–microbe homeostasis remains fragmented (12–14). Earlier studies indicated that 1) specific sectors of the plant innate immune system, namely phytohormones, have a role in sculpting root microbiota assemblages (15–17); 2) host responses to the root microbiota and environmental stresses are connected through the innate immune system to promote plant health (18–20); and 3) innate immune outputs are needed for accommodation and beneficial activities of model rhizobacterial strains and fungal root symbionts (21–25). Particularly, tryptophan (Trp)-derived, specialized metabolites were previously shown to represent key molecules necessary for microbe-mediated plant growth promotion in monoassociation experiments with *A. thaliana* (23–25).

The interplay between the plant innate immune system and the plant microbiota recently emerged as a key mechanism that maintains host–microbe homeostasis for plant health (13, 26–30). Dysbiosis is characterized by a disruption of this equilibrium caused by an imbalance in the microbiota, which in turn directly affect plant health. For instance, *A. thaliana* mutants simultaneously defective in PTI and the MIN7 vesicle-trafficking pathway (involved in modulating an aqueous microenvironment in the apoplast) or the membrane attack complex/perforin domain protein were shown to harbor abnormal, dysbiotic endosphere bacterial leaf microbiota assemblages. These host genetic networks, therefore, represent key molecular components controlling bacteria–host homeostasis in the phyllosphere (31, 32). In roots, however, the extent to which PTI also contributes to the maintenance and the regulation of the

Significance

Understanding how host–microbe homeostasis is controlled and maintained in plant roots is key to enhance plant productivity. However, the factors that contribute to the maintenance of this equilibrium between plant roots and their multikingdom microbial communities remain largely unknown. Here, we observed a link between fungal load in roots and plant health, and we showed that modulation of fungal abundance is tightly controlled by a two-layer regulatory circuit involving the host innate immune system on one hand and bacterial root commensals on another hand. Our results shed a light into how host–microbe and microbe–microbe interactions act in concert to prevent dysbiosis in *Arabidopsis thaliana* roots, thereby promoting plant health and maintaining growth-promoting activities of multikingdom microbial commensals.

Author contributions: S.H. designed research; K.W.W., B.P., S.G., A.P., and M.P.-B. performed research; K.W.W., N.V., T.T., and P.B. analyzed data; R.T.N., Y.B., and P.B. contributed new reagents/analytic tools; and K.W.W. and S.H. wrote the paper.

The authors declare no competing interest.

This article is a PNAS Direct Submission.

[1]To whom correspondence may be addressed. Email: hacquard@mpipz.mpg.de.

This article contains supporting information online at http://www.pnas.org/lookup/suppl/doi:10.1073/pnas.2111521118/-/DCSupplemental.

Published December 1, 2021.

symbiotic homeostasis remains unclear, especially in the context of complex multikingdom microbiomes.

Recent evidence indicates that microbial interactions, involving secretion of antimicrobial compounds or competition for nutritional resources dictate pathogen success in plant roots (33–36) and leaves (37, 38). Furthermore, microbiota reconstitution experiments with germ-free plants and diverse microbiota members isolated from roots of healthy *A. thaliana* revealed that cross-kingdom interactions in a synthetic root microbiome were critical for controlling diversity and composition of filamentous eukaryotes at the root interface, thereby promoting plant survival (39). Taken together, a current hypothesis is that microbial homeostasis in plant roots is controlled by both host–microbe and microbe–microbe interactions (40). However, the relative contribution of these two distinct outputs in maintaining homeostatic relationships between the plant and its root commensals needs to be determined.

Here, we tested the extent to which various *A. thaliana* immune sectors affect diversity, structure, and beneficial outcomes of a synthetic yet representative multikingdom root microbiome. We hypothesized that this machinery has not exclusively evolved as a surveillance system that terminates pathogen growth but rather as a microbial management system that maintains host–microbiota homeostasis for plant health. We provide evidence that at least one branch of the *A. thaliana* innate immune system involving Trp-derived, specialized metabolites is necessary for selectively controlling fungal load in plant roots, thereby preventing dysbiosis and maintaining growth-promoting outcomes of the multikingdom root microbiota. We also report that bacterial commensals are equally as important as these immune outputs in preventing fungal dysbiosis, underlining the importance of host- and bacterium-encoded mechanisms for maintaining homeostatic plant–microbiota interactions in roots, where bacteria and fungi cooccur.

Results

Intact Innate Immune System Is Needed for BFO-Mediated Plant Growth Promotion. We hypothesized that specific, host immune sectors might be necessary for beneficial, growth-promoting activities of microbial root commensals. In the gnotobiotic FlowPot system (39, 41), we recolonized germ-free *A. thaliana* Columbia-0 (Col-0, referred to as wild type [WT]) as well as a wide range of immunocompromised mutants with a synthetic multikingdom microbial community representative of naturally occurring root microbiomes (183 bacteria [B], 25 fungi [F], and 6 oomycetes [O]; BFO synthetic microbial community [SynCom], *SI Appendix*, Fig. S1 and Dataset S1) (3). The mutants include *bak1*/*bkk1* (42), *bak1*/*bkk1*/*cerk1* (31), *efr*/*fls2*/*cerk1* (43), *lyk5* (44), *apex* (45), and two other mutants (*hub1* and *hub2*) lacking hub proteins in the Leucine-rich repeat receptor kinases network with putative immunomodulatory functions (45), *wrky33*/*40* (46), *dde2*/*ein2*/*pad4*/*sid2* - *deps* (47), *pad4* (48), *cyp79b2*/*b3* (49), 35S::BRI1 (50), *bri1-301* (51), and *rar1* (52) (Fig. 1*A* and Dataset S2). Consistent with previous work (39), the BFO SynCom significantly promoted shoot fresh weight (FW) compared to germ-free control plants 5 wk post-BFO inoculation in the FlowPot system (*t* test, $P = 1.2e$ to 10; Fig. 1*B*). Notably, living microbes were needed for this plant growth–promoting activity, since heat-killed BFO SynCom members no longer promoted plant growth in this gnotobiotic system (*SI Appendix*, Fig. S2*A*). To analyze mutant-specific growth changes induced by the presence of the root microbiota, we first calculated the amplitude of the BFO effect between colonized and sterile plants for each genotype (mutants and WT; *SI Appendix*, Fig. S2*B*) and then normalized these differentials to that observed for WT (relative growth promotion, Kruskal–Wallis and Dunn control test with Bonferroni correction, Fig. 1*C*, see *Materials and Methods*). Remarkably, the vast majority of tested immunocompromised mutants (i.e., 64%) lost the ability to benefit from the multikingdom BFO SynCom (*bak1*/*bkk1*, *bak1*/*bkk1*/*cerk1*, *lyk5*, *wrky33*/*40*, *wrky33*, *pad4*, *cyp79b2*/*b3*, 35S::BRI1, *rar1*; Fig. 1*C*), indicating that several immune sectors were necessary for plant growth–promoting activities of microbial root commensals. It is noteworthy that several of these mutants also showed a growth defect relative to the WT control when grown in the Cologne agricultural soil (CAS) under greenhouse conditions, whereas this effect was not observed under sterile conditions (5 wk, *bak1*/*bkk1*, *wrky33*/*40*, *cyp79b2*/*b3*, 35S::BRI1, and *rar1*; *SI Appendix*, Figs. S2*B* and S3*A*). The results indicate a link between plant innate immune pathways and maintenance of beneficial plant–microbiota interactions.

Root Microbiota Composition Does Not Explain Variation in BFO-Mediated Plant Growth Promotion across Genotypes. We hypothesized that lack of BFO-mediated plant growth promotion in several of the immunocompromised mutants observed in the FlowPot system was associated with abnormal signatures in root microbiota composition. We harvested peat bulk soil, as well as roots of WT and mutant plants 5 wk post-BFO inoculation and monitored microbial community diversity and composition using amplicon sequencing of the bacterial 16S ribosomal RNA (rRNA) gene (B, 799F-1192R primers) and the fungal and oomycete internal-transcribed spacer (ITS, F: ITS1F-ITS2 primers, O: ITS1O-5.8sO primers). Alpha diversity analyses based on different metrics (Shannon index, Chao index, and observed 'operational taxonomic units' [OTUs]) did not reveal major effects of the different immune sectors on bacterial, fungal, and oomycete diversity in root samples (Fig. 2*A* and *SI Appendix*, Fig. S4). Constrained principal coordinate analysis (cPCoA) based on Bray–Curtis dissimilarities between samples revealed an overall significant yet subtle effect of the genotype on bacterial and fungal community composition in roots (B: 5.89%, $P = 0.001$; F: 7.62; $P = 0.001$, O: $P = 0.145$; Fig. 2 *D* and *E*), which was corroborated by permutational ANOVA (PERMANOVA, B: $R^2 = 0.033$; $P = 0.013$; F: $R_2 = 0.078$. $P = 0.002$; O: $R^2 = 0.084$, $P = 0.03$; Dataset S3). Further inspection of pairwise differences between WT and individual, immunocompromised mutants using cPCoA revealed significant differences in community composition for 6 out of 15 genotypes for bacteria (*hub1*, *hub2*, *bri1-301*, *wrky33*, *bak1*/*bkk1*/*cerk1*, and *cyp79b2*/*b3*) and only 1 out of 15 genotypes for fungi (*bri1-301*) and oomycetes (*wrky33*) (ANOVA, $P < 0.05$; Fig. 2 *D–F* and Dataset S4). Consistent with this, a genotype effect was only significant for bacterial community composition when the same mutants were grown in the CAS soil under greenhouse condition (B: 8.82%, $P = 0.001$; F: $P = 0.525$, O: $P = 0.051$), with bacterial assemblages in roots of the *hub1*, *cyp79b2*/*b3*, *efr*/*fls2*/*cerk1*, *wrky33*/*40*, *deps*, *rar1*, and *pad4* mutants differing significantly compared to the WT control (ANOVA, $P < 0.05$; *SI Appendix*, Fig. S3 *B–D*). We next tested whether differentiation in root microbiota composition detected across the different genotypes in the FlowPot system could explain the observed variation in BFO-mediated plant growth promotion (*SI Appendix*, Fig. S5). Using linear regression models, we did not detect significant associations between relative growth promotion indices (mean relative FW of colonized versus sterile genotypes; see Fig. 1*C*) and community differentiation measured along the first and second axis of the principal coordinate analysis ($n = 15$, $P > 0.05$ for bacteria, fungi, and oomycetes; *SI Appendix*, Fig. S5). Consistently, genotype-dependent changes in microbial assembly with respect to WT were only subtle at strain-level resolution (edgeR, generalized linear model, $P < 0.05$; *SI Appendix*, Fig. S6). Our results suggest that inactivation of specific immune sectors mildly

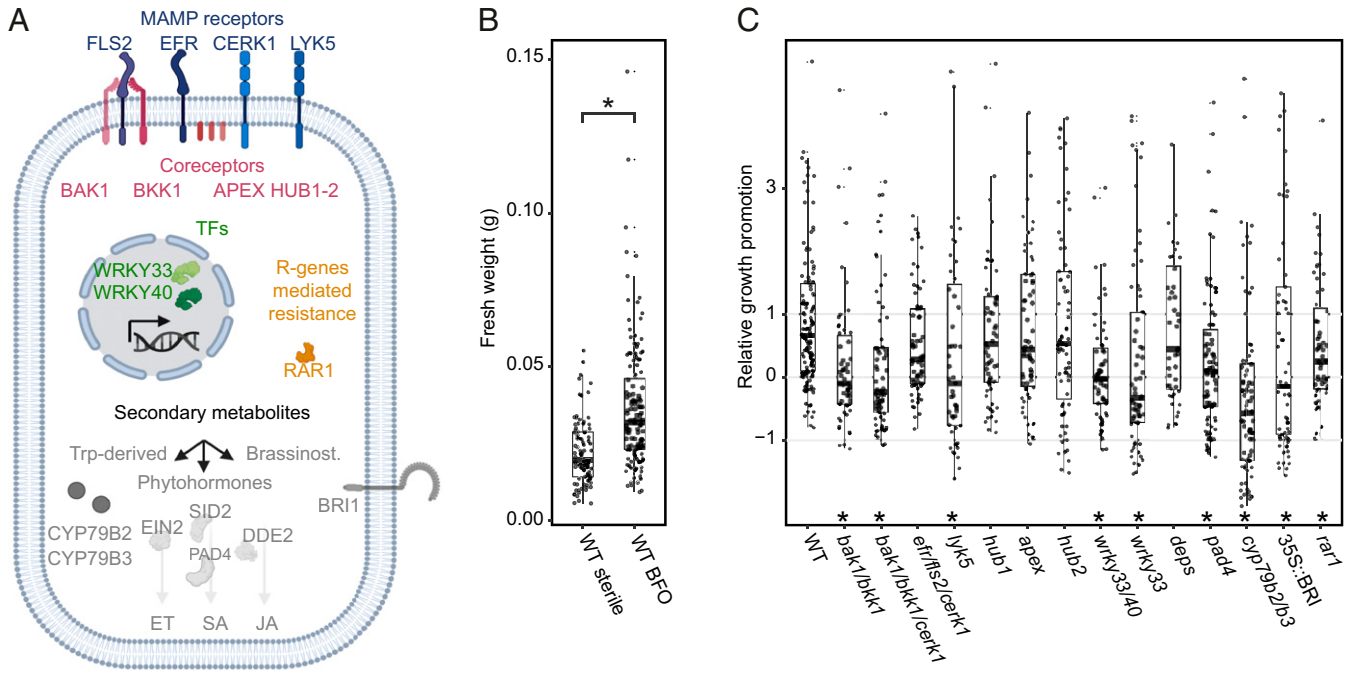

Fig. 1. A link between innate immunity and BFO-mediated plant growth promotion. (*A*) Schematic representation of investigated genes. (*B*) FW comparison between sterile and BFO-inoculated WT plants. *t* test, $*P < 0.05$, $n = 132$ plants for the BFO condition. (*C*) The relative growth promotion index was calculated by first subtracting the average sterile FW of each mutant from corresponding FW of BFO-treated plants and then by dividing this value by the average difference between BFO-treated and sterile WT (respective WT for each mutant). $n = 48$ to 132 plants per condition. Data comes from three independent biological replicates, with an exception for WT and *cyp79b2/b3* mutant, in which, in total, six biological replicates were performed. Significant differences were calculated using Kruskal–Wallis and Dunn control test with Bonferroni correction ($\alpha = 0.05$) based on transformed FW data. A total of 22 outliers with values above five are not shown on the graph for clarity reasons but were retained in the statistical analysis (*SI Appendix*, Fig. S2*C*).

sculpt microbial assemblages in roots and that genotype-specific differences in the composition of the root microbiota are unlikely the primary cause driving variation in BFO-mediated plant growth promotion across mutants.

Fungal Load in Roots Explains Variation in BFO-Mediated Plant Growth Promotion across Genotypes. We hypothesized that total microbial abundance in roots, rather than shifts in microbial community composition, might explain variation in BFO-mediated plant growth promotion in the FlowPot system. Using the same root samples used for microbial community profiling, we quantified bacterial, fungal, and oomycete load relative to the plant DNA marker gene *UBQ10* by qPCR (Fig. 3 *A–C* and Dataset S5). Specificity of all primer pairs was tested and cross-kingdom primer amplification was only observed between bacterial and plant DNA for the 799F-1192R primer pair. However, dilution series of pure bacterial DNA mixed with a fixed concentration of plant DNA indicated a linear amplification of the bacteria 16S rRNA gene, therefore suggesting a limited influence of plant DNA on bacterial quantification measurements (*Materials and Methods* and *SI Appendix*, Fig. S7). We detected significant, mutant-specific differences in bacterial and fungal but not oomycete load in plant roots with respect to WT (Kruskal–Wallis and Dunn control test with Bonferroni correction, $P < 0.05$; Fig. 3 *A–C*). Roots of the *bak1/bkk1* mutant had a significantly higher bacterial load than WT control plants (Fig. 3*A*), whereas those of the *efr/fls2/cerk1*, *wrky33*, and *cyp79b2/b3* mutants showed extensive fungal colonization (Fig. 3*B*). Inspection of fungal load in roots of the mutants grown in the CAS soil under greenhouse conditions revealed that the fungal load was the highest in the *efr/fls2/cerk1*, *cyp79b2/b3*, and *lyk5* mutants, although the differences were not significant among genotypes (*SI Appendix*, Fig. S3 *E* and *F*). To determine whether total microbial load can more precisely explain variation in BFO-mediated plant growth promotion across mutants observed in the FlowPot system (see Fig. 1*C*), we employed a similar linear regression model as described above (Fig. 3 *D–F*). Remarkably, increase in fungal, but not bacterial or oomycete load in plant roots, was significantly correlated with lack of BFO-mediated plant growth promotion ($n = 15$, $R^2 = 0.4196$, $P = 0.005374$; Fig. 3*E*). Notably, these differences in fungal load measured across genotypes explained 42% of the between-genotype variation in BFO-mediated plant growth promotion (Fig. 3*E*). The results suggest that control of fungal load in plant roots by independent immune sectors is key for maintaining the beneficial activity of the multikingdom BFO SynCom.

Trp-Derived Camalexin, Indole Glucosinolates, and IAA Are Individually Dispensable for Preventing Fungal Dysbiosis in Roots. Based on above-mentioned experiments, we observed that inactivation of two functionally redundant genes required to convert Trp into indole-3-acetaldoxime (IAOx, *CYP79B2* and *CYP79B3*) (49) was sufficient to shift a beneficial plant–microbiota association from a homeostatic state into a dysbiotic state (Fig. 1*C*). IAOx is precursor of several types of known Trp derivatives, including indole glucosinolates (IGs), with their hydrolysis products, and camalexin and indole-3-carboxylic acids (ICAs), whose accumulation was strongly compromised in roots of *cyp79b2/b3* plants grown in the FlowPot system, as compared with WT plants (*SI Appendix*, Fig. S8*A*). We also observed that levels of free indole-3-acetic acid (IAA, auxin) were significantly reduced with respect to WT, partly recapitulating reductions observed for CYP79B2/B3-dependent metabolites (*SI Appendix*, Fig. S8*B*). This is consistent with previous results observed for the same mutant but in leaves and at temperatures that were higher [26 °C (49)] than those measured inside our FlowPot system (i.e., oscillating between 18.9 °C, light phase, and 24.3 °C, dark

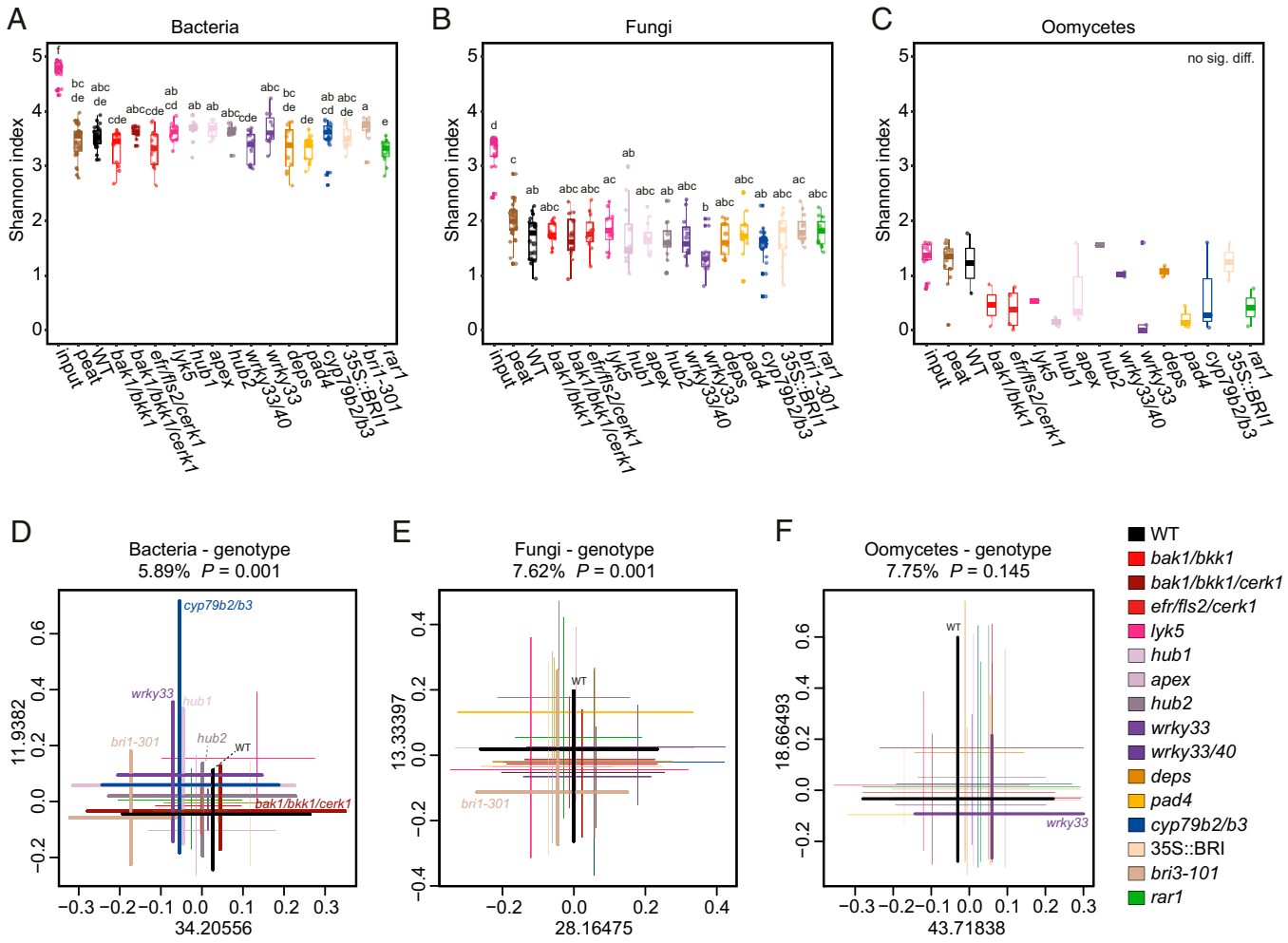

Fig. 2. Subtle shifts in root microbiota composition across immunocompromised mutants. (*A–C*) Alpha diversity Shannon index for bacterial (*A*), fungal (*B*), and oomycetes (*C*) communities. "Input" refers to initial microbial pool at T0, whereas "peat" corresponds to an unplanted pot containing peat and the BFO SynCom only. Significant differences were calculated using Kruskal–Wallis and Dunn test ($\alpha = 0.05$). The number of samples per condition are the following: bacteria: $n = 11$ to 28, fungi: $n = 11$ to 28, and oomycetes: $n = 1$ to 18. (*D–E*) cPCoA, based on Bray–Curtis distances, constrained by "genotype" for bacterial (*D*), fungal (*E*), and oomycetes (*F*) communities. Each cross covers the minimal and maximal values per axis of the respective genotype. The number of samples per condition are the following: bacteria: bacteria: $n = 11$ to 28 (cut off 1,000 reads), fungi: $n = 9$ to 28 (cut off 1,000 reads), and oomycetes: $n = 5$ to 27 (cut off 100 reads). Percentage value above the graph represents the variance explained by the genotype effect. Genotypes significantly different from WT (ANOVA, $P < 0.05$, see Dataset S4) are highlighted with thick lines and their respective genotypes names are highlighted on the graphs.

phase; *SI Appendix*, Fig. S9). In contrast, levels of CYP79B2/B3-independent metabolites, such as aliphatic glucosinolates, flavonoids, coumarins, and phenolic acids did not vary significantly between *cyp79b2/b3* and WT in root samples (*SI Appendix*, Fig. S8*C*), confirming the specific impact of *cyp79b2/b3* mutations on Trp derivatives in roots of plants used in our experiments. We tested the extent to which the different branches of Trp metabolism could contribute to the maintenance of fungal homeostasis in roots and the BFO-mediated plant growth promotion using a set of mutants that, according to the literature, should be defective in the accumulation of camalexin [*pad3* (53), *cyp71a27* (25), and *cyp71a12/a13* (54)], ICAs [*cyp71a12/a13* (54)], IGs [*myb34/51/122* (55)], and some of their hydrolysis products [*pen2* (56) and *pyk10/bglu21* (57)] (*SI Appendix*, Fig. S10*A* and Dataset S2). By repopulating these mutants and WT plants with the BFO SynCom in the gnotobiotic FlowPot system, we observed that none of the tested mutants phenocopied plant growth (*SI Appendix*, Fig. S10 *B* and *C*) and fungal load (*SI Appendix*, Fig. S10 *D–F*) phenotypes observed in the context of the *cyp79b2/b3* mutant. To validate deficiency of tested lines in the accumulation of particular metabolites, we analyzed their accumulation in roots of these mutants inoculated with the fungal pathogen *Plectosphaerella cucumerina*, a species that is widespread in *A. thaliana* roots (3) and present in our fungal SynCom. This analysis proved lack of camalexin in roots of *pad3* and *cyp71a12/a13* lines as well as IG deficiency in *myb34/51/122* mutant (*SI Appendix*, Fig. S11); however, it did not confirm partial ICA deficiency observed earlier in infected leaves of *cyp71a12/a13* plants (58). Strikingly, we also found a *cyp79b2/b3*-like reduction in free IAA levels in roots of *myb34/51/122* plants, which indicated that in *A. thaliana* roots significant amounts of this hormone can be derived from IAOx through IGs, as already postulated (59). Collectively, our metabolic analysis, combined with results on fungal load (*SI Appendix*, Fig. S10 *D–F*) and plant growth promotion (*SI Appendix*, Fig. S10 *B* and *C*), excluded individual contributions of IAA, IGs, and camalexin but not of ICAs to fungal overgrowth in *cyp79b2/b3* plants.

Dysbiotic Phenotype of the *cyp79b2/b3* Mutant Is Retained at the Reproductive Stage. To test the robustness of the dysbiotic phenotype (i.e., increased fungal load and altered plant growth)

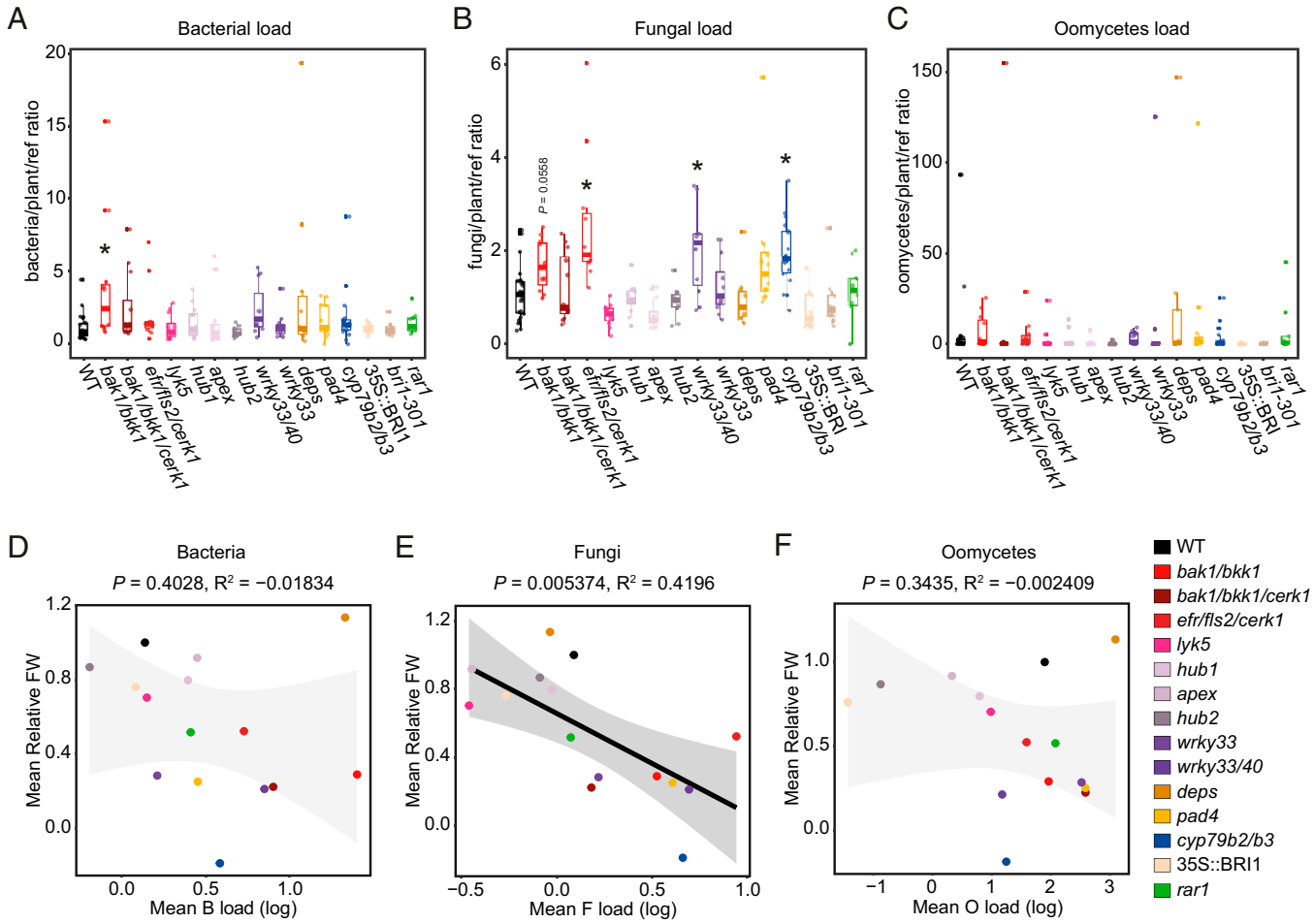

Fig. 3. Fungal load in roots explains BFO-mediated plant growth phenotypes. (*A–C*) Bacterial (*A*), fungal (*B*), and oomycetes (*C*) load in plant root samples, calculated based on qPCR data relative to plant UBQ10 reads. Asterisks indicate genotypes that were significantly different from WT. Significant differences were calculated using Kruskal–Wallis and Dunn control test with Bonferroni correction ($\alpha = 0.05$) and WT as a control. The number of samples per condition are the following: bacteria: $n = 10$ to 23, fungi: $n = 11$ to 24, and oomycetes: $n = 10$ to 23. (*D–F*) Linear regression between mean bacterial (*D*), fungal (*E*), and oomycetes (*F*) load and mean plant relative FW (i.e., mean relative plant growth promotion index), *P* value, and R^2 were obtained from ANOVA ($n = 15$ genotypes).

during the plant life cycle, we adapted our gnotobiotic FlowPot system to accommodate plant growth for up to 8 wk until reproductive stage and production of the first siliques (see *Materials and Methods* and *SI Appendix*, Fig. S12). By repopulating roots of WT and *cyp79b2/b3* genotypes with the BFO SynCom, we observed that plant dry weight of the *cyp79b2/b3* mutant was significantly reduced compared to sterile plants 8 wk post-BFO inoculation (Kruskal–Wallis and Dunn test with Bonferroni correction), which was not the case for WT plants (Fig. 4*A*; see BFO WT versus BFO *cyp79b2/b3)*. Consistent with the aforementioned results obtained at the vegetative stage (Figs. 1*C* and 3*B*), variation in BFO-induced differential growth between WT and *cyp79b2/b3* at the reproductive stage was associated with increased root fungal but not bacterial load (Fig. 4 *D–F*; see BFO WT versus BFO *cyp79b2/b3*) and changes in bacterial but not fungal community composition between the two genotypes (Fig. 4 *G* and *H*; see BFO WT versus BFO *cyp79b2/b3*). These results were validated by PERMANOVA (Dataset S6; see model BFO, genotype effect, B: $R^2 = 0.1685$, $P = 0.001$, F: $R^2 = 0.068$, $P = 0.249$). Our results indicate that the striking dysbiotic phenotype observed for the *cyp79b2/b3* mutant at the vegetative stage was retained at the reproductive stage, irrespective of difference in residence time (vegetative stage: 5 wk and reproductive stage: 8 wk) and growth conditions (vegetative stage: light cabinet and reproductive stage: greenhouse). Notably, high fungal load and BFO-induced growth penalty observed in this mutant, compared to WT control plants, were not associated with significant differences in bolting time, number of first siliques produced per living plant (Fig. 4 *B* and *C*; see BFO WT versus BFO *cyp79b2/b3*), or other tested parameters (*SI Appendix*, Fig. S13), suggesting that the living plants harvested 8 wk post-BFO inoculation showed penalty on growth rather than on these initial indicators of reproductive fitness.

Trp Metabolism and Bacterial Root Commensals Control Fungal Load to Promote Plant Survival. We previously showed that bacterial root commensals modulate fungal diversity and composition at the root interface, thereby promoting *A. thaliana* survival in the gnotobiotic FlowPot system (39). Therefore, we also tested the extent to which bacterial commensals and host Trp metabolism act in concert to modulate fungal growth in plant roots to promote *A. thaliana* health.

In the above-mentioned experiment conducted at the reproductive stage, we also recolonized roots of WT and *cyp79b2/b3* genotypes with all possible combinations of single- and multi-kingdom microbial consortia (B, F, O, BO, BF, and FO). We observed that F, O, and FO communities negatively impacted

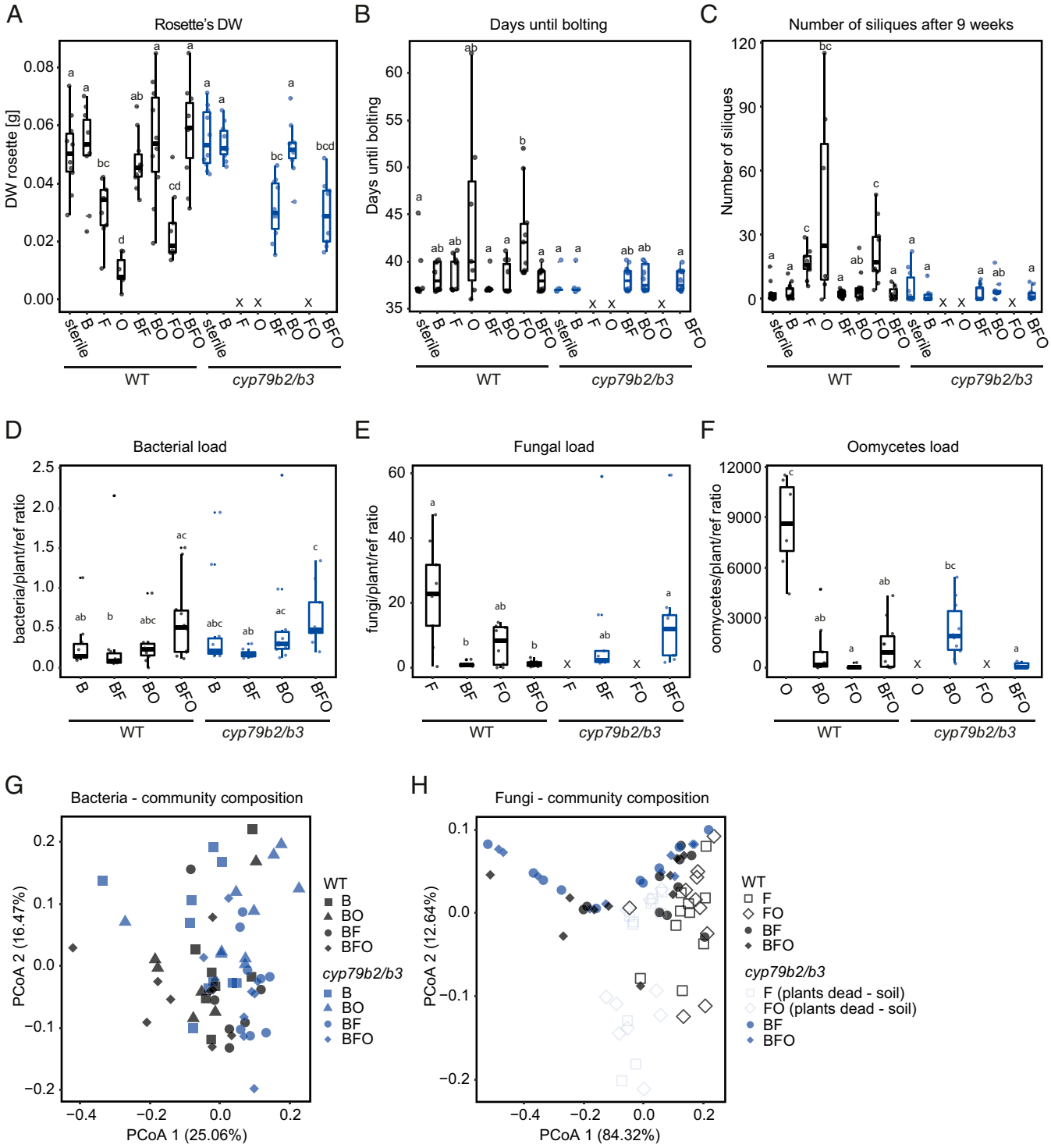

Fig. 4. Trp metabolism and bacterial commensals prevent fungal dysbiosis in roots. (*A*) Statistical differences of rosette's dry weight (DW) were calculated with ANOVA and Tukey's post hoc test ($\alpha = 0.05$). (*B*) Days until bolting significant differences were calculated using Kruskal–Wallis and Dunn test with Bonferroni correction ($\alpha = 0.05$). (*C*) Statistical differences in siliques numbers were calculated using Kruskal–Wallis and Dunn test with Bonferroni correction ($P < 0.05$). *(A–C)* $n = 0$ to 10 samples per condition. (*D–F*) Total bacterial (*D*), fungal (*E*), and oomycetes (*F*) abundance in the roots of 9-wk-old plants. Statistical differences for total microbial abundance were calculated using Kruskal–Wallis and Dunn test with Bonferroni correction ($\alpha = 0.05$). The number of samples per condition are the following: bacteria: $n = 11$ to 15, fungi: $n = 0$ to 15, and oomycetes: $n = 0$ to 15. (*G* and *H*) PCoA based on Bray–Curtis distances between samples for bacterial (*G*) and fungal (*H*) community. The number of samples per condition are the following: bacteria: $n = 8$ to 15 and fungi: $n = 6$ to 15.

the dry weight of WT plants (Fig. 4*A*) and triggered, in most cases, early bolting and silique production compared to the sterile control condition (Fig. 4 *B* and *C*). Dramatic consequences on growth, survival, and reproductive fitness were observed for the *cyp79b2/b3* mutant since none of the plants survived in the absence of the bacterial community (see

crosses in Fig. 4 *A–C* and *SI Appendix*, Fig. S13). In contrast, bacterial root commensals alone were not detrimental for the growth of both WT and *cyp79b2/b3* genotypes (B WT and B *cyp79b2/b3*) and were able to fully rescue *cyp79b2/b3* rosette dry weight to control level in the presence of oomycetes (*cyp79b2/b3*, O versus BO condition) but not when fungi were present in the SynComs (*cyp79b2/b3*, B versus BF and B versus BFO conditions, $P < 0.05$, ANOVA and Tukey's post hoc test) (Fig. 4*A*). These results indicate that the presence of fungi rather than oomycetes or bacteria in the BFO SynCom was likely the cause of the dysbiotic phenotype observed for this mutant (Fig. 4*A*). Importantly, a similar experiment conducted at the vegetative stage with individual microbial groups or their combinations showed the same results, thereby strengthening this conclusion (*SI Appendix*, Fig. S14). Furthermore, we also assembled a second independent fungal SynCom using strains that were previously isolated from roots of *A. thaliana* harvested in a natural population in Saint-Dié, France (39), for repopulation experiments in the FlowPot system (F^{sd}: 23 members; Dataset S1). Although F^{sd} was less detrimental on plant growth than the original F SynCom, the fungal effect on WT and *cyp79b2/b3* significantly differed in the absence of bacterial root commensals ($P < 0.05$, Kruskal–Wallis test and Dunn test; *SI Appendix*, Fig. S15), validating the hypersusceptibility of the *cyp79b2/b3* mutants to at least two independent fungal communities isolated from geographically distant environments.

To determine how bacterial commensals supplement Trp metabolism to prevent fungal dysbiosis, we next inspected microbial load (qPCR; Fig. 4 *D–F*), as well as microbial diversity and microbial community composition in plant roots (amplicon sequencing; Fig. 4 *G* and *H* and *SI Appendix*, Fig. S16). Given that the *cyp79b2/b3* mutant did not survive treatments with fungi only, we inspected these signatures in the context of WT plants. We observed that the presence of bacterial commensals led to a significant reduction in fungal load in plant roots (Kruskal–Wallis and Dunn test with Bonferroni correction, $P < 0.05$; Fig. 4*E*) but not diversity (Kruskal–Wallis and Dunn test, $P > 0.05$; *SI Appendix*, Fig. S16 *A–C*), as well as a dramatic shift in fungal community composition (Fig. 4*H* and *SI Appendix*, Fig. S16*E*) compared to conditions in which these fungi were inoculated in the absence of bacteria (see F versus BF conditions). These differences in fungal community composition in the presence of bacteria were corroborated by PERMANOVA (Dataset S6; global model, Treatment: F: $R^2 = 0.287$, $P = 0.001$). Taken together, the results indicate that modulation of fungal load by the host Trp metabolism and of fungal composition and fungal load by bacterial root commensals are both necessary and act additively to prevent fungal dysbiosis in *A. thaliana* roots.

Discussion

Here, we observed that maintenance of fungal–host homeostasis in *A. thaliana* roots is needed for microbiota-induced plant growth promotion in a community context. Plant innate immune outputs and bacterial biocontrol capabilities were identified as key factors acting in concert to maintain homeostatic relationships between plant roots and their multikingdom microbial commensals. Our results suggest that fungal growth suppression by immune outputs in roots is necessary for *A. thaliana* health but is nonetheless insufficient to fully prevent fungal burden in the absence of bacterial root commensals. Our results illustrate that host-encoded immune functions and bacterium-encoded protective activities have likely complemented each other's over evolutionary time to promote balanced root colonization by beneficial multikingdom microbial communities.

Consistent with previous reports (15–17, 20), we observed that the composition of root-associated bacterial communities was significantly altered in several immunocompromised mutants, validating that diverse immune sectors differentially sculpt root bacterial assemblages in nature (13, 14). However, we observed that these differences were subtle and that genotype-specific differences in bacterial community composition were not sufficient to explain variation in microbiota-induced differences in growth phenotypes. These results suggest that the plant innate immune system is robust and that functional redundancies and compensatory mechanisms likely occur to prevent bacterial dysbiosis in plant tissues (60). Consistent with that, recent studies reported that coinactivation of several host genetic components was needed to cause dysbiosis in the *A. thaliana* phyllosphere (31, 32). These results nonetheless indicate that the plant innate immune system is a key machinery that links phyllosphere microbial community composition to plant health.

Although we used a set of mutants impaired in responses to both bacterial and fungal pathogens, we observed that the composition of the bacterial root microbiota was affected by inactivation of diverse immune sectors more extensively than that of fungal communities. In sharp contrast, the relative fungal load in roots was modulated by innate immune outputs more extensively than the bacterial load. We speculate that the differential control of microbial load and assembly by the host immune system is relevant for the accommodation of multikingdom microbial consortia. This result might reflect the fact that phylogenetically diverse, *A. thaliana* root–colonizing fungi display higher pathogenic potential than that of root-derived bacteria in monoassociation with the host (27, 39, 61–63) and show more extensive, site-specific associations with *A. thaliana* roots than bacteria in nature (3). Furthermore, the reciprocal and complex interplay between bacterial root commensals and PTI reported recently corroborated that PTI outputs selectively modulate bacterial assembly, which in turn instructs the host immune system (13, 14, 64, 65). Notably, a subset of bacterial root commensals was found to suppress a specific and evolutionarily conserved sector of the *A. thaliana* immune system, and cooccurrence of suppressive and nonsuppressive isolates in the root microbiome appears to be critical for the maintenance of host–microbial homeostasis (27, 29).

By screening several immunocompromised plants in a gnotobiotic plant system, we observed that a large majority of the mutants showed a significant reduction in BFO-mediated plant growth promotion compared to the WT control. Therefore, an intact immune system is needed for the plant growth–promoting outcome of multikingdom microbial root commensals. A link between fungal load in roots and plant performance has been previously suggested in monoassociation experiments with fungal root endophytes (23, 62). Inspection of a diverse set of *A. thaliana* root mycobiota members revealed that fungal colonization aggressiveness and detrimental effect on plant performance are correlated and suggested that the most beneficial fungi are less abundant than detrimental fungi in roots of natural *A. thaliana* populations (62). Furthermore, *A. thaliana* mutants impaired in Trp-derived, specialized metabolites were shown to be unable to control growth and accommodation of beneficial fungal root endophytes, which likely contributed to the altered plant growth phenotypes (23, 24, 66). Our results obtained in a community context are consistent with this previous work, since inactivation of two redundant genes encoding cytochrome P450 enzymes, required to convert Trp into IAOx (*CYP79B2* and *CYP79B3*), was sufficient to induce fungal dysbiosis in a microbial community context, thereby turning a beneficial multikingdom SynCom into a detrimental SynCom.

The prominent effect of Trp-derived on fungal load rather than on fungal community composition is consistent with the observation that growth of the *cyp79b2/b3* mutant was

previously shown to be impaired upon colonization by phylogenetically diverse beneficial and pathogenic root–colonizing fungi (23, 24, 67–71). Our observation that two fully independent fungal SynComs containing unrelated fungal taxa (F and F^{sd}) having both detrimental effect on the growth and survival of the *cyp79b2/b3* mutant further corroborates this conclusion. However, a targeted screen with additional mutants impaired specifically in the production of camalexin or IGs did not reveal a causal link with fungal dysbiosis. We were not able to validate putative contribution of ICAs, because of the fact that, unlike reported in infected leaves, *cyp71a12/a13* mutant appeared to accumulate WT-like levels of these compounds in roots. Lack of *cyp79b2/b3*-like phenotypes in tested metabolic mutants is potentially explained by the observation that known Trp derivatives form a redundant multilayer system (58) and that only simultaneous removal of all of them might result in a clear dysbiosis phenotype. Notably, our metabolic analysis of *cyp79b2/b3* and *myb34/51/122* mutants indicated that considerable pools of free IAA in *A. thaliana* roots can be derived from IAOx via indol-3-ylmethyl glucosinolate. However, despite the fact that impaired auxin signaling and reduced auxin levels in *A. thaliana* leaves were shown to associate with increased susceptibility to necrotrophic fungal pathogens (72), phenotypes of *myb34/51/122* mutant excluded that fungal load and associated dysbiotic state observed in roots of the *cyp79b2/b3* mutant is dependent exclusively on IAA deficiency. This is in line with a recent report on *A. thaliana* and the beneficial fungal root endophyte *Colletotrichum tofieldiae*, which indicated that the IG-dependent route for auxin biosynthesis was dispensable for the outcome of this mutualistic interaction (73). Additional work is needed to identify the exact molecular components downstream CYP79B2 and CYP79B3 that modulate fungal homeostasis in *A. thaliana* roots and to determine the extent to which this pathway is evolutionarily conserved beyond *A. thaliana* and related *Brassicaceae* species.

It remains difficult to experimentally test whether bacterial commensals and Trp-derived secondary metabolites, identified here as key factors preventing fungal dysbiosis in our gnotobiotic plant system, remain important under natural conditions. Our results from the greenhouse experiment using the natural CAS soil indicate important, quantitative differences in the outputs measured across genotypes (plant growth, community composition, and microbial load) but also notable similarities. The growth penalty and the high fungal load observed for *cyp79b2/b3* mutant, as well as the significant difference in bacterial, but not fungal community composition observed in roots of the *cyp79b2/b3* versus WT were highly consistent, irrespective of differences in soil matrix, microbiota diversity/composition, and growth conditions. However, although the fungal load was high in roots of the *cyp79b2/b3* mutant, differences with the other genotypes were less pronounced than that observed in the FlowPot system, suggesting that biotic or abiotic factors other than those manipulated in the FlowPot system might also contribute the maintenance of fungal–host homeostasis when plants are grown in the CAS soil under seminatural conditions.

We conclude that control of fungal homeostasis in *A. thaliana* roots is key for host health in a gnotobiotic plant system, and we provide evidence that the maintenance of a symbiotic homeostasis is not only controlled by plant-encoded mechanisms but also by bacteria-encoded functions that likely supplement the host innate immune system in nature.

Materials and Methods

All experiments were performed at least three times independently, except experiments at the reproductive stage that were performed two times independently because of the longer timeframe (9 wk).

***A. thaliana* Mutant Lines.** In this study, a total of 23 *A. thaliana* lines were used. *A. thaliana* Col-0 was used as a WT, together with 22 mutants in the Col-0 background (Dataset S2).

Greenhouse Experiment. Natural soil experiment was performed in the greenhouse in short day conditions (8-h light) in 9 × 9 cm square pots filled with natural CAS soil. Plants were grown for 5 wk, and the pots were randomized weekly within biological replicates. Around ∼2 wk after sowing, the extra seedlings were removed and only five plants were left per pot.

Preparation of Synthetic Microbial Communities. A total of 183 bacterial strains isolated from healthy *A. thaliana* roots (20, 74) were grown for 7 d in 600 μL 50% tryptic soy broth liquid media from a glycerol stock. A total of 100 μL of each strain was taken, combined together, centrifuged, and the pellet was resuspended in 10 mM $MgCl_2$. A total of 25 fungal and 6 oomycetes strains were grown individually on potato glucose agar media for 2 wk and harvested 1 d before the experiments (20). Harvested F and O mycelium (average of 50 mg/strain) was suspended in 1 mL 10 mM $MgCl_2$ inside a sterile 2-mL screwcap tube containing one stainless steel bead (3.2-mm diameter) and left at 4 °C overnight. On the day of the experiment, the mycelium was crushed for 10 min in a paint shaker (SK450, Fast & Fluid Management). A similar protocol was used to prepare the second fungal SynCom. Bacterial, fungal, and oomycete strains used in this study can be found in *SI Appendix*, Fig. S1 and Dataset S1. Note that over the course of experiments two oomycetes strains (namely 210 and 29) did not survive, and so, they were only used in the initial screen of innate immunity mutants.

FlowPot Preparation and Growth Conditions.

Vegetative stage experiment. FlowPots were prepared as described before (39, 41) with six FlowPots per microbox (SacO2, TD3000 + TPD3000, 3 L volume). Each FlowPot was repopulated with 200 μL bacterial, 200 μL fungal, and 80 μL oomycete pools, and each sterile FlowPot was mock inoculated with 480 μL 10 mM $MgCl_2$ (to account for the solution used to resuspend microbial cultures) and placed in light cabinets (Versatile Environmental Test Chamber MLR-352, Panasonic) with 10 h light (luminous flux per unit area inside the growth chamber average 9627.929, inside Microboxes average 6992.714). Temperature was set at 21 °C during the light period and 19 °C during the dark period. Seeds were sterilized by rotating at 40 rpm for 15 min in 70% ethanol, centrifuged for 1 min at 1,000 rpm in order to remove 70% ethanol, quickly washed with 100% ethanol, and immediately followed by another centrifugation step (1 min, 1,000 rpm). Afterward, the seeds were dried under the sterile bench, suspended in sterile water, and left in the dark at 4 °C for 2 to 3 d. Around 1 wk after sowing six seeds per FlowPot, extra seedlings were removed under sterile conditions, leaving a maximum of four plants per FlowPot. Plants were harvested after 5 wk of growth. All sterile soil samples were plated on 50% tryptic soy agar plates to check for possible contaminations. If a true contamination was discovered, the samples originating from the contaminated box were removed from further analysis. All treatments lacking bacteria were also checked to confirm the lack of bacterial contamination. Note that sterile controls for the *bri1-301* mutant always showed contamination resulting from an endophytic bacterium residing in the seeds, and, therefore, no sterile FW data were shown for this mutant. This mutant was therefore excluded from the analyses shown in Figs. 1*C* and 3 *D–F* and *SI Appendix*, Fig. S5.

Reproductive stage experiment. The general procedure of FlowPots preparation is the same as for vegetative stage, with few main differences. FlowPots were prepared from the same 50/60-mL syringes but cut at the 45-mL mark instead of 25 mL. FlowPots were placed in a custom-made metal rack, instead of a plastic one inside a big microbox (SacO2 category No. TP 5000 + TPD 5000, 5 L volume) that was covered with a lid for the first 5 wk of growth (*SI Appendix*, Fig. S12). Afterward, the lid was exchanged with another 5l microbox placed upside down to allow accommodation of the flowering stem in the last 4 wk of growth (*SI Appendix*, Fig. S12). Two boxes were held together with 5-cm–wide micropore tape (3 M, category No. 1530–2). Plants were grown in the greenhouse: first, in short day conditions (8-h light) for 3 wk and then, on an open table supplemented with light (16-h light) for another 6 wk, resulting in 9 wk of growth in total. Around 2 wk after sowing, germination/early survival rate was scored, and extra seedlings were removed under sterile conditions, leaving one plant per FlowPot. During that time, individual FlowPots were watered with ∼4 mL one-half Murashige and Skoog (MS) media. After 5 wk of growth (during an exchange of the lid), plants were watered again with the same amount of sterile one-half MS media. Boxes were randomized on a weekly basis within their respective biological replicates and dates of bolting, and first flower and silique formation were scored on a daily basis for each plant individual. Similar to vegetative stage experiment,

soil samples from sterile treatments were taken to validate sterility. All treatments lacking bacteria were also checked to confirm the lack of bacterial contamination.

Calculation of Relative Growth Promotion across Mutants in the FlowPot System. To calculate the relative growth promotion index (Fig. 1*C* and *SI Appendix*, Fig. S10*C*), the first step was to compute the difference in shoot FW between BFO and sterile conditions per genotype (i.e., FW_{BFO} – mean $FW_{sterile}$). This allows to account for genotype-specific differences in vegetative growth. In this first step of the calculation, values will be above zero if there is a growth promotion and below if the growth is restricted compared to sterile conditions. Because the experiment was done in two batches, these differential growth values measured for WT and mutants were all normalized to that of WT by dividing them with the mean differential, observed in the WT context. For WT, this normalization resulted in a mean relative growth promotion value of 1. However, note that in the boxplots depicted in Fig. 1*C* and *SI Appendix*, Fig. S10*C*, the median is shown, not the mean.

Heat-Kill FlowPot Control Experiment. Methodology of this experiment was the same as for vegetative stage experiment, with the use of only WT and an addition of "heat-kill" treatment. Heat-kill treatment was performed by taking the fully assembled BFO SynCom (prepared as described above) and subjecting it to two subsequent rounds of autoclaving (20 min at 121 °C for each round). Each FlowPot from heat-kill treatment was inoculated with 200 μL heat-killed bacterial, 200 μL heat-killed fungal, and 80 μL heat-killed oomycete communities.

Harvesting.

Greenhouse. Rosettes of all plants (maximum of 5) were cut and their FW measured. Roots were washed in sterile MQ water three times, then once in detergent (1%Tris-EDTA [TE] + 0.1% Triton X-100), once in 70% ethanol, once in 3% bleach, and again three times in sterile MQ water, following the fractionation protocol described before (39). Afterward, the roots were dried shortly on the paper filter and frozen in Lysing E matrix tubes (MP Biomedicals) in liquid nitrogen. Soil samples were taken from unplanted pots: First, a top 2-cm layer of soil was removed, and ∼1 g soil was taken from the middle of the pot into Lysing E matrix tube and immediately frozen in liquid nitrogen. Samples were stored in −80 °C until further processing.

Vegetative stage experiment. Rosettes of all plants were cut and their FW was measured. Four representative FlowPots were chosen from each box, and their roots were harvested for microbiome analysis in the following way. Roots were washed four times in sterile MQ water, dried shortly on a paper filter, and flash frozen in Lysing E matrix tubes (MP Biomedicals) in liquid nitrogen. Samples were stored in −80 °C until further processing. Experiment was repeated at least three times independently, giving a total of up to 12 replicates per treatment.

Reproductive stage experiment. First, the chlorophyll content index (CCI) (Opti-Sciences Chlorophyll Content Meter CCM-200) was measured. For each plant, three randomly selected leaves from the middle of the rosette were measured, and each of these leaves was measured twice to account for possible measurement variation. Two technical measurements per leaf were averaged, and later, three averaged values from each plant were averaged again in order to obtain a single, representative CCI value per plant. Next, the stem was cut, taped to a white sheet of A4 paper, had a picture taken, and then placed for 7 d in a bag in the 80 °C oven for dry weight measurements. Separately, rosette FW was measured and, similarly to stem, placed in the oven for dry weight measurements. Stem pictures were later used to count the total number and length of the main stem, number of branching points, and number of siliques. Experiment was repeated twice, with up to five technical replicates per experiment (one replicate being an individual plant), giving a total of up to 10 replicates per genotype × treatment combination.

DNA Extraction and Library Preparation. DNA was isolated with FastDNA Spin Kit for Soil (MP Biomedicals) following the manufacturer's instructions. Library for sequencing followed the protocol described in ref. 39. In short, after DNA isolation, DNA samples were diluted to 5 ng/μL based on PicoGreen measurements (Quant-iT PicoGreen dsDNA Assay-Kit, Invitrogen) and amplified in a two-step PCR with primers amplifying the bacterial 16S rRNA V5-V7 region (799F-1192R) and the fungal and oomycete ITS1 (fungi: ITS1F-ITS2 and oomycetes: ITS1O-5.8sO) (see ref. 39). Amplified bacterial products were purified on 1.5% agarose gel with QIAquick Gel Extraction Kit (Qiagen, category No. 28704) and fungal and oomycetes products with Agencourt AMPure XP beads (Beckman Coulter, category No. A63882). After purification, single bacterial, fungal, and oomycetes samples were pooled together within their respective microbial groups in equimolar concentrations, cleaned again with Agencourt AMPure XP beads, and finally pooled together into one final microbial library sample. Final pooling of bacterial, fungal, and oomycetes samples varied between 300 and 850 ng per microbial group, depending on the availability of the samples.

Sequencing Data Analysis. Prepared libraries were sequences on a MiSeq machine with pair-end Illumina sequencing (MiSeq reagent Kit v3, 600 cycle, category No. MS-102-3003). Primers used for sequencing are as described previously in ref. 39. Quality filtered and demultiplexed sequencing reads were mapped at 98% identity to the reference sequence database for bacteria, fungi, and oomycete using usearch (75). Unmapped reads were discarded. Count tables were derived from this mapping. Samples used for further analysis were filtered with the threshold of minimum 1,000 reads per sample for all microbiota-dependent analysis.

Measurement of Microbial Load in Plant Roots. Primers tested for specificity are listed in Dataset S5. Tests for specificity were performed with the same PCR protocol used for amplicon library preparation [PCR I (39)]. Primers amplifying the *A. thaliana UBQ10* showed the highest-primer efficiency and no signs of cross-amplification. Primers amplifying the bacterial 16S rRNA gene (V5-V7 region, 799F-1192R), and the fungal and oomycete ITS1 (fungi: ITS1F-ITS2, oomycetes: ITS1O-5.8sO) were chosen with the main advantage of being the same primer pairs used for microbial community profiling (Dataset S5). Subsequent PCR tests revealed that fungal and oomycetes primers are fully specific to their respective synthetic communities. Bacteria primers, although cross-amplifying the plant 16S rRNA gene, show a strong preference for bacterial DNA, since Cq readout was highly correlated with increase of bacterial load, regardless of the varying presence of plant DNA (*SI Appendix*, Fig. S7). Note that at least one oomycete strain used in our SynCom was colonized by a hyphae-associated bacterium, causing an unspecific cross-amplification with the primers used to amplify the bacterial 16S rRNA gene. The qPCR protocol as follows: 95 °C for 3 min, 40 cycles (95 °C for 15 s, 60 °C for 30 s, and 72 °C for 30 s), 95 °C for 10 s, and melting curve measurement from 55 °C to 95 °C with an increment of 0.5 °C. The total microbial load (relative to *UBQ10*) was calculated with the use of the following formula. Analysis includes one reference sample present on each plate in technical triplicates, serving as an interpolate normalization (named ref. in below formula).

$$x = ((2\text{^}(-C_q\text{ITS1})/2\text{^}(-C_q\text{UBQ10})))/2\text{^}(-C_q\text{ref}).$$

***P. cucumerina* Infections Assay.** MS medium with 1% Agar (BioShop) and 0.5 mM MES, pH 5.7, was poured into 120 × 120 mm square GREINER plates, and a 2-cm slide was cut out of the plates. Stratified sterile *Arabidopsis* seeds were imbibed in 10 mM $MgCl_2$ for 48 h in and transferred on the edge of the removed agar slide (10 seeds/plate). The plates were kept under short day conditions in PANASONIC MLR-352-PE phytochamber, as described earlier (73). Roots of 4-wk-old seedlings were spray inoculated with spore suspension (4×10^6 spores/mL) of adapted Brigitte Mauch-Mani (BMM) isolate of *P. cucumerina* BMM. Around 48 h after inoculation, root samples (about 100 mg) were collected and frozen immediately in liquid nitrogen.

Liquid Chromatography–Mass Spectrometry Analysis. Frozen root samples were extracted with DMSO (Sigma-Aldrich) containing 0.5 mM camphorsulfonic acid and 0.5 mM lidocaine (Sigma-Aldrich), as described earlier (58). Samples were subjected to liquid chromatography–mass spectrometry (LC-MS) analyses performed using the UltiMate 3000 RS (Dionex, Thermo Fisher Scientific) attached to a TIMS-TOF mass spectrometer (Bruker Daltonics). Chromatographic separation was carried out on a BEH RP C18 column (2.1 × 150 mm, 1.7-μm particle size) at 30 °C with a mobile phase flow rate of 0.30 mL/min. The elution was conducted using water containing 0.1% formic acid (Sigma-Aldrich) (Solvent A) and acetonitrile (VWR Chemicals) containing 0.01% of formic acid (Solvent B) in the following gradient: 0 to 5 min from 10 to 30% B, 5 to 12 min to 100% B, 12 to 15 min maintained at 100% B, and up to 15.5 min the system was returned to starting conditions and reequilibrated for 5 min. The spectrometer was calibrated with sodium formate salt clusters prior to each analysis. MS was operated using the following settings: ion source voltage of −4.5 kV, nebulization of nitrogen at a pressure of 2.2 bar, and a gas flow rate of 10 L/min. Ion source temperature was 220 °C. The spectra were scanned in positive and negative ionization in fragmentation mode (data-dependent tandem mass spectrometry, ddMSMS) at a range of 95 to 1,000 *m/z* at a resolution >30,000 full width at half maximum (Dataset S7). Data acquisition was supervised by Compass HyStar version 5.1 software (Bruker Daltonics). Data were analyzed by Compass DataAnalysis version 5.3 (Bruker Daltonics). Data from both experiments, FlowPot and agar-based system, were processed separately by MS-Dial ver 4.24. Processing steps included conversion of raw LC-MS file to format suitable for MS-Dial software, transformation from profile to centroid data, peak detection, annotation to spectral MSMS public

metabolomic library, adduct elimination, alignment, and gap filling by compulsion (Dataset S8). IAA, camalexin, and ICA peaks were identified based on LC-MS analysis of respective standard compounds. Other metabolites were putatively identified based on their mass-to-charge ratio (*m/z* value) and fragmentation spectra.

Statistical Analyses. All statistical analyses were performed in R. Differences were considered as statistically significant when $P < 0.05$. For Kruskal–Wallis and Dunn test, FSA package was used, and for Dunn control test, PMCMR package was used. When the variables were normally distributed, the effect of the treatments and genotypes were assessed using linear models with ANOVA. Whenever necessary the response variable was root square or log transformed to ensure a normal distribution of the model's residuals.

The models were constructed as follows: $\mathrm{lm}(\log(\mathrm{bolt_{to}flower_{days}}) \sim \mathrm{genotype} * \mathrm{treatment})$.

Generalized linear models (GLMs) were used when the transformation did not successfully normalize the variable. An example of GLM model with gamma distribution is presented below:

$$\mathrm{mod} = \mathrm{glm}(\mathrm{days_{to}bolting} \sim \mathrm{treatment} * \mathrm{genotype},$$
$$\mathrm{family} = \mathrm{Gamma}\left(\mathrm{link} = \ddot{\log}\right))$$

Differential abundance of strains between WT and Mutants was calculated by normalization of raw sequencing counts (TMM normalization, "calcNormFactors" from R package "EdgeR") and fitting a generalized linear model ("glmFit") including the replicate effects. Significantly different microbial taxa were then determined with a likelihood ratio test ("glmRT," $P < 0.05$).

Variance partitioning between experiments, biological replicates, genotypes, and treatments were tested with a PERMANOVA approach with the Adonis function (R package vegan) in all experiments. For the root microbiota differentiation across mutants experiment, the effect of the genotype, the biological replicate, and the experimental replicate on microbial communities' composition were tested in a global model, including the soil samples and a second model without soil samples. These models were constructed separately on each of the bacterial and fungal datasets using Bray–Curtis dissimilarity matrices between pairs of samples produced with the vegdist function (R package vegan). For the WT versus *cyp79b2/b3* experiment, the effect of the genotype and treatment factors on microbial communities' composition were tested in a global model. The effect of the genotype was then tested in separated models for each treatment separately and for bacteria and fungi separately. These models where constructed using Bray–Curtis dissimilarity matrices between pairs of samples produced with the vegdist function (R package vegan).

Data Availability. Sequencing reads from microbiota reconstitution experiments (MiSEq. 16S rRNA and ITS reads) have been deposited in European Nucleotide Archive (ENA) PRJEB45520 for bacteria, PRJEB45521 for fungi, and PRJEB45522 for oomycetes. Sequencing reads from the greenhouse experiment (MiSEq. 16S rRNA and ITS reads) are also available at ENA (PRJEB47599 for bacteria, PRJEB47600 for fungi, and PRJEB47601 for oomycetes). All scripts for computational analysis and corresponding raw data are available at GitHub (https://github.com/ththi/Wolinska-et-al.-2021). All other study data are included in the article and/or supporting information.

ACKNOWLEDGMENTS. This work was supported by funds to S.H. from a European Research Council starting grant (MICRORULES 758003), the Max Planck Society, as well as the Cluster of Excellence on Plant Sciences, funded by the Deutsche Forschungsgemeinschaft. P.B. was supported by National Science Centre HARMONIA grant (UMO-2015/18/M/NZ1/00406). Y.B. is supported by grants from the Austrian Academy of Sciences through the Gregor Mendel Institute. We thank Dr. Kenichi Tsuda for providing *deps* and *pad4 A. thaliana* mutant lines, Dr. Jane Parker for *rar1*, and Prof. Stanislav Kopriva for the *cyp71a27*. We thank Karin Grunwald for helping in the isolation and selection of the *hub1* and *hub2* T-DNA lines. Finally, we thank Fantin Mesny, Jane Parker, Marcel Bucher, and Paul Schulze-Lefert for providing helpful comments regarding the manuscript or during departmental seminars and thesis advisory committee meetings. Portions of the paper were developed from the PhD thesis of K.W.W. (https://kups.ub.uni-koeln.de/35745/).

1. M. A. Hassani, P. Durán, S. Hacquard, Microbial interactions within the plant holobiont. *Microbiome* **6**, 58 (2018).
2. R. L. Berendsen, C. M. J. Pieterse, P. A. H. M. Bakker, The rhizosphere microbiome and plant health. *Trends Plant Sci.* **17**, 478–486 (2012).
3. T. Thiergart *et al.*, Root microbiota assembly and adaptive differentiation among European Arabidopsis populations. *Nat. Ecol. Evol.* **4**, 122–131 (2020).
4. C. R. Fitzpatrick *et al.*, The plant microbiome: From ecology to reductionism and beyond. *Annu. Rev. Microbiol.* **74**, 81–100 (2020).
5. J. D. G. Jones, J. L. Dangl, The plant immune system. *Nature* **444**, 323–329 (2006).
6. D. E. Cook, C. H. Mesarich, B. P. H. J. Thomma, Understanding plant immunity as a surveillance system to detect invasion. *Annu. Rev. Phytopathol.* **53**, 541–563 (2015).
7. H. Cui, K. Tsuda, J. E. Parker, Effector-triggered immunity: From pathogen perception to robust defense. *Annu. Rev. Plant Biol.* **66**, 487–511 (2015).
8. D. Couto, C. Zipfel, Regulation of pattern recognition receptor signalling in plants. *Nat. Rev. Immunol.* **16**, 537–552 (2016).
9. J.-M. Zhou, Y. Zhang, Plant immunity: Danger perception and signaling. *Cell* **181**, 978–989 (2020).
10. C. M. J. Pieterse, D. Van der Does, C. Zamioudis, A. Leon-Reyes, S. C. Van Wees, Hormonal modulation of plant immunity. *Annu. Rev. Cell Dev. Biol.* **28**, 489–521 (2012).
11. X. Yu, B. Feng, P. He, L. Shan, From chaos to harmony: Responses and signaling upon microbial pattern recognition. *Annu. Rev. Phytopathol.* **55**, 109–137 (2017).
12. C. Zipfel, G. E. Oldroyd, Plant signalling in symbiosis and immunity. *Nature* **543**, 328–336 (2017).
13. S. Hacquard, S. Spaepen, R. Garrido-Oter, P. Schulze-Lefert, Interplay between innate immunity and the plant microbiota. *Annu. Rev. Phytopathol.* **55**, 565–589 (2017).
14. P. J. P. Teixeira, N. R. Colaianni, C. R. Fitzpatrick, J. L. Dangl, Beyond pathogens: Microbiota interactions with the plant immune system. *Curr. Opin. Microbiol.* **49**, 7–17 (2019).
15. S. L. Lebeis *et al.*, PLANT MICROBIOME. Salicylic acid modulates colonization of the root microbiome by specific bacterial taxa. *Science* **349**, 860–864 (2015).
16. L. C. Carvalhais *et al.*, Linking jasmonic acid signaling, root exudates, and rhizosphere microbiomes. *Mol. Plant Microbe Interact.* **28**, 1049–1058 (2015).
17. R. F. Doornbos, B. P. J. Geraats, E. E. Kuramae, L. C. Van Loon, P. A. H. M. Bakker, Effects of jasmonic acid, ethylene, and salicylic acid signaling on the rhizosphere bacterial community of *Arabidopsis thaliana*. *Mol. Plant Microbe Interact.* **24**, 395–407 (2011).
18. G. Castrillo *et al.*, Root microbiota drive direct integration of phosphate stress and immunity. *Nature* **543**, 513–518 (2017).
19. S. Hacquard *et al.*, Survival trade-offs in plant roots during colonization by closely related beneficial and pathogenic fungi. *Nat. Commun.* **7**, 11362 (2016).
20. S. Hou *et al.*, A microbiota-root-shoot circuit favours *Arabidopsis* growth over defence under suboptimal light. *Nat. Plants* **7**, 1078–1092 (2021).
21. J. M. Plett *et al.*, Ethylene and jasmonic acid act as negative modulators during mutualistic symbiosis between *Laccaria bicolor* and Populus roots. *New Phytol.* **202**, 270–286 (2014).
22. B. Gourion, F. Berrabah, P. Ratet, G. Stacey, Rhizobium-legume symbioses: The crucial role of plant immunity. *Trends Plant Sci.* **20**, 186–194 (2015).
23. U. Lahrmann *et al.*, Mutualistic root endophytism is not associated with the reduction of saprotrophic traits and requires a noncompromised plant innate immunity. *New Phytol.* **207**, 841–857 (2015).
24. K. Hiruma *et al.*, Root endophyte Colletotrichum tofieldiae confers plant fitness benefits that are phosphate status dependent. *Cell* **165**, 464–474 (2016).
25. A. Koprivova *et al.*, Root-specific camalexin biosynthesis controls the plant growth-promoting effects of multiple bacterial strains. *Proc. Natl. Acad. Sci. U.S.A.* **116**, 15735–15744 (2019).
26. V. Chaudhry *et al.*, Shaping the leaf microbiota: Plant-microbe-microbe interactions. *J. Exp. Bot.* **72**, 36–56 (2021).
27. K.-W. Ma *et al.*, Coordination of microbe-host homeostasis by crosstalk with plant innate immunity. *Nat. Plants* **7**, 814–825 (2021).
28. Y. Song *et al.*, FERONIA restricts Pseudomonas in the rhizosphere microbiome via regulation of reactive oxygen species. *Nat. Plants* **7**, 644–654 (2021).
29. P. J. P. L. Teixeira *et al.*, Specific modulation of the root immune system by a community of commensal bacteria. *Proc. Natl. Acad. Sci. U.S.A.* **118**, e2100678118 (2021).
30. S. Pfeilmeier *et al.*, The plant NADPH oxidase RBOHD is required for microbiota homeostasis in leaves. *Nat. Microbiol.* **6**, 852–864 (2021).
31. X.-F. Xin *et al.*, Bacteria establish an aqueous living space in plants crucial for virulence. *Nature* **539**, 524–529 (2016).
32. T. Chen *et al.*, A plant genetic network for preventing dysbiosis in the phyllosphere. *Nature* **580**, 653–657 (2020).
33. Z. Wei *et al.*, Trophic network architecture of root-associated bacterial communities determines pathogen invasion and plant health. *Nat. Commun.* **6**, 8413 (2015).
34. Z. Wei *et al.*, Initial soil microbiome composition and functioning predetermine future plant health. *Sci. Adv.* **5**, eaaw0759 (2019).
35. S. Gu *et al.*, Competition for iron drives phytopathogen control by natural rhizosphere microbiomes. *Nat. Microbiol.* **5**, 1002–1010 (2020).
36. V. J. Carrión *et al.*, Pathogen-induced activation of disease-suppressive functions in the endophytic root microbiome. *Science* **366**, 606–612 (2019).
37. M. T. Agler *et al.*, Microbial hub taxa link host and abiotic factors to plant microbiome variation. *PLoS Biol.* **14**, e1002352 (2016).
38. K. Eitzen, P. Sengupta, S. Kroll, E. Kemen, G. Doehlemann, A fungal member of the *Arabidopsis thaliana* phyllosphere antagonizes *Albugo laibachii* via a GH25 lysozyme. *eLife* **10**, e65306 (2021).

39. P. Durán *et al.*, Microbial interkingdom interactions in roots promote *Arabidopsis* survival. *Cell* **175**, 973–983.e14 (2018).
40. F. Getzke, T. Thiergart, S. Hacquard, Contribution of bacterial-fungal balance to plant and animal health. *Curr. Opin. Microbiol.* **49**, 66–72 (2019).
41. J. M. Kremer *et al.*, Peat-based gnotobiotic plant growth systems for *Arabidopsis* microbiome research. *Nat. Protoc.* **16**, 2450–2470 (2021).
42. M. Roux *et al.*, The *Arabidopsis* leucine-rich repeat receptor-like kinases BAK1/SERK3 and BKK1/SERK4 are required for innate immunity to hemibiotrophic and biotrophic pathogens. *Plant Cell* **23**, 2440–2455 (2011).
43. D. C. Prince, C. Drurey, C. Zipfel, S. A. Hogenhout, The leucine-rich repeat receptor-like kinase BRASSINOSTEROID INSENSITIVE1-ASSOCIATED KINASE1 and the cytochrome P450 PHYTOALEXIN DEFICIENT3 contribute to innate immunity to aphids in *Arabidopsis*. *Plant Physiol.* **164**, 2207–2219 (2014).
44. Y. Cao *et al.*, The kinase LYK5 is a major chitin receptor in *Arabidopsis* and forms a chitin-induced complex with related kinase CERK1. *eLife* **3**, e03766 (2014).
45. E. Smakowska-Luzan *et al.*, An extracellular network of *Arabidopsis* leucine-rich repeat receptor kinases. *Nature* **553**, 342–346 (2018).
46. S. Liu, B. Kracher, J. Ziegler, R. P. Birkenbihl, I. E. Somssich, Negative regulation of ABA signaling by WRKY33 is critical for *Arabidopsis* immunity towards *Botrytis cinerea* 2100. *eLife* **4**, e07295 (2015).
47. K. Tsuda, M. Sato, T. Stoddard, J. Glazebrook, F. Katagiri, Network properties of robust immunity in plants. *PLoS Genet.* **5**, e1000772 (2009).
48. J. Glazebrook *et al.*, Phytoalexin-deficient mutants of *Arabidopsis* reveal that PAD4 encodes a regulatory factor and that four PAD genes contribute to downy mildew resistance. *Genetics* **146**, 381–392 (1997).
49. Y. Zhao *et al.*, Trp-dependent auxin biosynthesis in *Arabidopsis*: Involvement of cytochrome P450s CYP79B2 and CYP79B3. *Genes Dev.* **16**, 3100–3112 (2002).
50. Y. Belkhadir *et al.*, Brassinosteroids modulate the efficiency of plant immune responses to microbe-associated molecular patterns. *Proc. Natl. Acad. Sci. U.S.A.* **109**, 297–302 (2012).
51. W. Xu, J. Huang, B. Li, J. Li, Y. Wang, Is kinase activity essential for biological functions of BRI1? *Cell Res.* **18**, 472–478 (2008).
52. P. Tornero *et al.*, RAR1 and NDR1 contribute quantitatively to disease resistance in *Arabidopsis*, and their relative contributions are dependent on the R gene assayed. *Plant Cell* **14**, 1005–1015 (2002).
53. J. Glazebrook, F. M. Ausubel, Isolation of phytoalexin-deficient mutants of *Arabidopsis thaliana* and characterization of their interactions with bacterial pathogens. *Proc. Natl. Acad. Sci. U.S.A.* **91**, 8955–8959 (1994).
54. T. M. Müller *et al.*, Transcription activator-like effector nuclease-mediated generation and metabolic analysis of camalexin-deficient cyp71a12 cyp71a13 double knockout lines. *Plant Physiol.* **168**, 849–858 (2015).
55. H. Frerigmann *et al.*, Regulation of pathogen-triggered tryptophan metabolism in *Arabidopsis thaliana* by MYB transcription factors and indole glucosinolate conversion products. *Mol. Plant* **9**, 682–695 (2016).
56. V. Lipka *et al.*, Pre- and postinvasion defenses both contribute to nonhost resistance in *Arabidopsis*. *Science* **310**, 1180–1183 (2005).
57. A. J. Nagano *et al.*, Quantitative analysis of ER body morphology in an *Arabidopsis* mutant. *Plant Cell Physiol.* **50**, 2015–2022 (2009).
58. M. Pastorczyk *et al.*, The role of CYP71A12 monooxygenase in pathogen-triggered tryptophan metabolism and *Arabidopsis* immunity. *New Phytol.* **225**, 400–412 (2020).
59. S. K. Malka, Y. Cheng, Possible interactions between the biosynthetic pathways of indole glucosinolate and auxin. *Front Plant Sci* **8**, 2131 (2017).
60. Y. Kim *et al.*, Mechanisms underlying robustness and tunability in a plant immune signaling network. *Cell Host Microbe* **15**, 84–94 (2014).
61. C. Junker, S. Draeger, B. Schulz, A fine line–Endophytes or pathogens in *Arabidopsis thaliana*. *Fungal Ecol.* **5**, 657–662 (2012).
62. F. Mesny *et al.*, Genetic determinants of endophytism in the *Arabidopsis* root mycobiome. *Nat. Commun.*, 10.1038/s41467-021-27479-y (2021).
63. O. M. Finkel *et al.*, A single bacterial genus maintains root growth in a complex microbiome. *Nature* **587**, 103–108 (2020).
64. K. Parys *et al.*, Signatures of antagonistic pleiotropy in a bacterial flagellin epitope. *Cell Host Microbe* **29**, 620–634.e9 (2021).
65. N. R. Colaianni *et al.*, A complex immune response to flagellin epitope variation in commensal communities. *Cell Host Microbe* **29**, 635–649.e9 (2021).
66. P. L. Nongbri *et al.*, Indole-3-acetaldoxime-derived compounds restrict root colonization in the beneficial interaction between *Arabidopsis* roots and the endophyte *Piriformospora indica*. *Mol. Plant Microbe Interact.* **25**, 1186–1197 (2012).
67. D. J. Kliebenstein, H. C. Rowe, K. J. Denby, Secondary metabolites influence *Arabidopsis*/*Botrytis* interactions: Variation in host production and pathogen sensitivity. *Plant J.* **44**, 25–36 (2005).
68. A. Sanchez-Vallet *et al.*, Tryptophan-derived secondary metabolites in *Arabidopsis thaliana* confer non-host resistance to necrotrophic *Plectosphaerella cucumerina* fungi. *Plant J.* **63**, 115–127 (2010).
69. H. U. Stotz *et al.*, Role of camalexin, indole glucosinolates, and side chain modification of glucosinolate-derived isothiocyanates in defense of *Arabidopsis* against *Sclerotinia sclerotiorum*. *Plant J.* **67**, 81–93 (2011).
70. K. Hiruma *et al.*, Glutathione and tryptophan metabolism are required for *Arabidopsis* immunity during the hypersensitive response to hemibiotrophs. *Proc. Natl. Acad. Sci. U.S.A.* **110**, 9589–9594 (2013).
71. A. Muñoz-Barrios *et al.*, Differential expression of fungal genes determines the lifestyle of *Plectosphaerella* strains during *Arabidopsis thaliana* colonization. *Mol. Plant Microbe Interact.* **33**, 1299–1314 (2020).
72. F. Llorente *et al.*, Repression of the auxin response pathway increases *Arabidopsis* susceptibility to necrotrophic fungi. *Mol. Plant* **1**, 496–509 (2008).
73. H. Frerigmann, M. Piotrowski, R. Lemke, P. Bednarek, P. Schulze-Lefert, A network of phosphate starvation and immune-related signaling and metabolic pathways controls the interaction between *Arabidopsis thaliana* and the beneficial fungus *Colletotrichum tofieldiae*. *Mol. Plant Microbe Interact* **34**, 560–570 (2021).
74. Y. Bai *et al.*, Functional overlap of the *Arabidopsis* leaf and root microbiota. *Nature* **528**, 364–369 (2015).
75. R. C. Edgar, Search and clustering orders of magnitude faster than BLAST. *Bioinformatics* **26**, 2460–2461 (2010).